Chemical Geology 273 (2010) 168–179

Contents lists available at ScienceDirect

Chemical Geology

journal homepage: www.elsevier.com/locate/chemgeo

# Tracing fluid–rock reaction and hydrothermal circulation at the Saldanha hydrothermal field

Á.S. Dias [a,*], R.A. Mills [b], I. Ribeiro da Costa [a], R. Costa [a,c], R.N. Taylor [b], M.J. Cooper [b], F.J.A.S. Barriga [a]

[a] CREMINER, Department of Geology, University of Lisbon, Ed. C6, Piso4, Campo Grande, 1749-016 Lisboa, Portugal
[b] School of Ocean and Earth Science, National Oceanography Centre, Southampton, University of Southampton, SO14 3ZH, UK
[c] EMEPC, R. Costa Pinto 165, 2770-070 Paço-de-Arcos, Portugal

ARTICLE INFO

*Article history:*
Received 15 May 2009
Received in revised form 29 December 2009
Accepted 16 February 2010

Editor: B. Bourdon

*Keywords:*
Saldanha hydrothermal field
Radiogenic isotopes
Steatization

ABSTRACT

The Saldanha hydrothermal field is positioned on the top of a seamount located in a non-transform offset (NTO5) on the Mid-Atlantic Ridge (MAR). This hydrothermal system was first described as a low-temperature diffuse field, driven by peridotite–seawater reactions following the detection of high concentrations of $CH_4$ and $H_2$ in the water column, and the occurrence of serpentinite outcrops in the vent area. We have studied the geochemistry and isotopic composition of sediment and rock samples collected across the area and show that hydrothermal circulation at Saldanha is complex and spatially variable, comprising areas of low-temperature diffuse flow but also more focused higher-temperature venting zones. While most sediment samples have an isotopic composition that is similar to normal pelagic sediments, one core (SCD7) show significant hydrothermal influence, sulphide mineralization, non-radiogenic Pb and radiogenic Nd isotope ratios and positive Eu anomalies. This is best explained by mineral precipitation from high-temperature hydrothermal fluids that have circulated through mafic rocks. The host rock lithology and alteration is also highly variable and comprises both fresh basalts, serpentinites and hydrothermally altered rocks (metabasalts, metagabbros and steatites). Serpentinites have REE patterns and $\varepsilon_{Nd(0)}$ values that fall between seawater and mantle peridotite reference values, resulting from extensive interaction of seawater with the original peridotite. This process was probably favoured by the deeply penetrating and long-lived faults occurring at this NTO. Steatites have a positive Eu anomaly and non-radiogenic Pb isotopic values. These signatures, together with the sulphide mineralisation and the extensive Si input necessary for steatization of serpentinites, imply that higher-temperature hydrothermal fluids reacted with gabbroic intrusions at depth. The more hydrothermally altered sediment and rock samples appear to be associated with the Saldanha fault network that promotes a more focused fluid flow and thus enhances hydrothermal alteration within a region of low-temperature diffuse flow.



## 1. Introduction

Hydrothermal activity associated with ultramafic outcrops at mid-ocean ridges (MOR) is a relatively recent discovery. This type of activity seems to be confined to slow and ultraslow spreading ridges and the ultramafic outcrops are usually associated with detachment faulting, low magma budgets, relatively thin crust and irregular faulting patterns (Cannat et al., 1997; Gràcia et al., 2000; Mevel, 2003).

The first evidence for this type of activity on the Mid-Atlantic Ridge (MAR) was the discovery of the Logatchev field (Krasnov et al., 1995) followed by the Rainbow field (Fouquet et al., 1997), both hosting high-temperature hydrothermal activity. Other ultramafic-hosted systems discovered later on the MAR include the low-temperature Saldanha (Barriga et al., 1998) and Lost City fields (Kelley et al., 2001). The detection of $H_2$ and $CH_4$ anomalies in the overlying water column, resulting from the serpentinization of abyssal peridotites (e.g. Charlou et al., 2002; Seyfried et al., 2007), suggests that these types of hydrothermal systems are common (Charlou et al., 1993; German et al., 1996; Charlou et al., 2002). The dynamics of the hydrothermal processes driving these systems is still poorly known and in particular their heat source has been the source of some debate. However in low-temperature ultramafic-hosted hydrothermal systems the heat source has been suggested to be derived from the exothermic reactions of serpentinization (e.g. Barriga et al., 1998; Kelley et al., 2001; Lowell and Rona, 2002; Schroeder et al., 2002), through heat balance models suggest that an additional heat source is necessary particularly for higher-temperature fields such as Rainbow and Logatchev (Lowell and Rona, 2002; Allen and Seyfried, 2004).

The Saldanha hydrothermal field is hosted in ultramafic and mafic rocks and it is located on a 100 m high semi-circular NNE–SSW seamount (2200–2300 m deep) within a non-transform offset (NTO5), between the Famous and Amar segments (36° 34′N; 33° 26′W) on the Mid-Atlantic Ridge (MAR) (Fig. 1). This site was first visited by the Nautile submersible in 1998 (Barriga et al., 1998). The discovery of

* Corresponding author. Tel.: +351 217500000.
*E-mail address:* agata.dias@fc.ul.pt (Á.S. Dias).

0009-2541/$ – see front matter © 2010 Elsevier B.V. All rights reserved.
doi:10.1016/j.chemgeo.2010.02.020

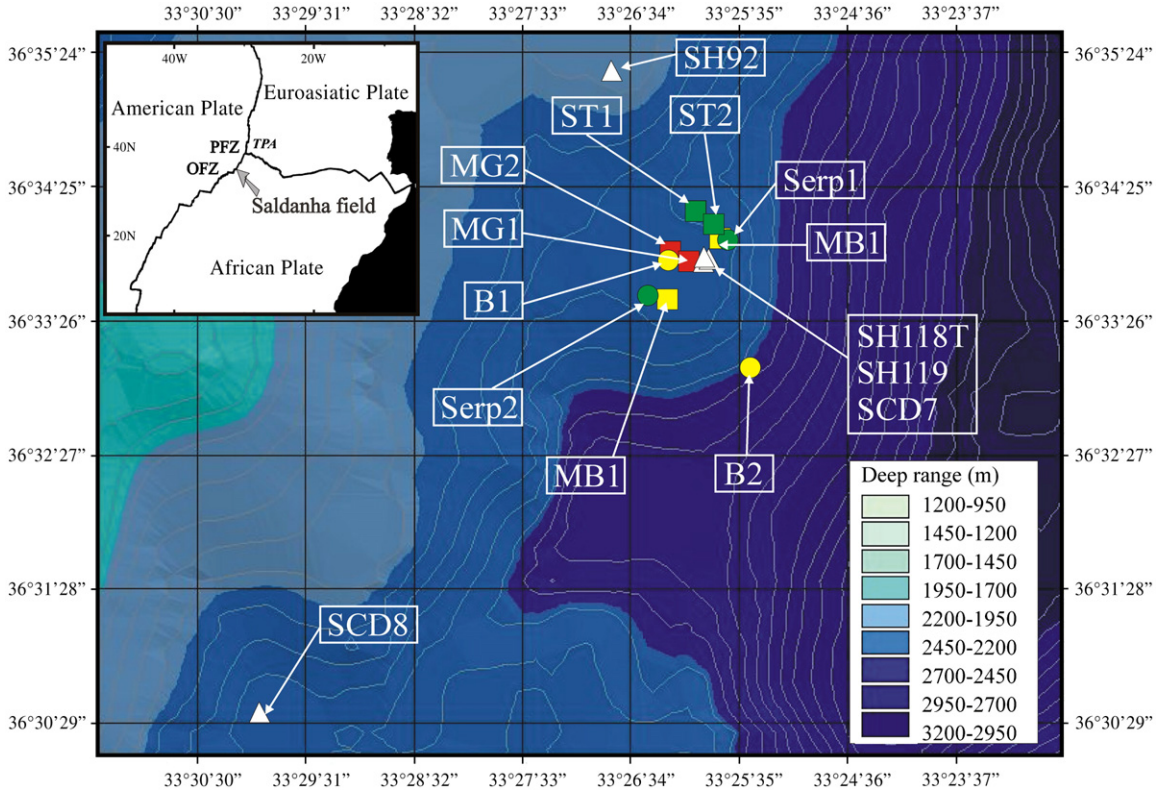


**Fig. 1.** Location of the Saldanha hydrothermal field and the sediment and rock samples used in this study. Legend: Δ Sediment cores (SH; SCD); ● Basalts (B); ■ Metabasalts (MB): ■ Metagabbros (Mg); ● Serpentinites (Serp); ■ Steatites (ST).

diffuse venting confirmed the presence of hydrothermal activity related to serpentinization processes, which had been inferred from the detection of geochemical anomalies in the water column (Charlou et al., 1997; Bougault et al., 1998).

Hydrothermal activity occurs essentially as diffuse flow, but more focused activity also takes place through centimetre sized holes in the sediments (Dias and Barriga, 2006). Temperatures measured few centimetres above the vent orifices by the ROV Victo during the Seahma (Seafloor and Sub-seafloor Hydrothermal Modelling in the Azores Sea) mission in 2001 were less than 9 °C (Barriga et al., 2003). The measured temperatures are lower than the end-member fluid temperature due to the mixing of the hydrothermal fluid with the surrounding cooler (2 °C) seawater. Petrographic and geochemical studies of sediments from this vent area, collected by a gravity core during CD167 in 2004, reveal that hydrothermal fluids have reacted with these sediments at temperatures higher than 250 °C, and suggest that fluids flowing through these sediments reach the surface at much higher-temperatures than those recorded during the SEAHMA mission (Dias et al., submitted for publication).

Direct observations during dives and identification of samples collected in the area revealed the presence of highly heterogeneous lithologies across the Saldanha massif. At the top of the seamount, basalts, metasomatized gabbros and basalts, serpentinites and steatites (talc-bearing serpentinites) were identified and sampled during the Flores'96, Saldanha'98 and Sehama'02 missions (Barriga et al., 1998; Fouquet et al., 1998; Barriga et al., 2003). Steatites are located essentially at the northern part of the Saldanha dome in a NE–SW elongated area. This is most probably related to a dominant fault network striking NE–SW, E–W and WNW–ESE, responsible for the exposure of ultramafic rocks and which seems to play an important role in hydrothermal circulation at this site (Gràcia et al., 2000). Around the Saldanha seamount fresh basalts are the dominant lithology, except at the base of the SW flank where a significant outcrop of serpentinized peridotite exposed by a NE–SW discontinuity occurs, and on the NE flank where gabbroic rocks also outcrop in a scarping fault with the same orientation as the serpentinites.

To further understand the hydrothermal processes generating the Saldanha hydrothermal field, REE concentrations and the Nd and Pb isotope composition of sediments and host rocks from the Saldanha hydrothermal field were determined. These data allow quantification of the relative contributions of seawater and hydrothermal fluids to the altered basement rocks and also the discrimination of hydrothermal and other sources for the sediments. Combining rock and sediment isotopic data also allows the fluid–rock–sediment interaction, in particular the contributions of mafic- and ultramafic-rocks to the fluid chemistry to be discerned, which is ultimately reflected in the hydrothermal signature recorded in sediments.

## 2. Sampling and analytical methods

Sediment cores were collected from the Saldanha hydrothermal field during Seahma'02 (Barriga et al., 2003) and Charles Darwin — CD167 (Sinha et al., 2006) missions in 2002 and 2004, respectively. During the Seahma'02 mission samples were collected with ROV-Victor using short push-cores (40 cm). During CD167 samples were collected with a gravity corer. In this study, Seahma samples are identified with a SH prefix and CD167 samples with a SCD prefix. Five sediment cores were selected for analyses, three collected in the area of active venting (SH119, SH118T and SCD7) and two collected from a background area (SCD8 and SH92) (Table 1). Down core geochemical analyses were performed for all samples except for SH118T. This sample was capped by a Fe–Mn oxide crust and the upper centimetre of the sediment was recovered with a ROV spade after crust removal. The sediment was mixed during recovery and bulk analyses for this sample were made separately from the oxide crust.

Rock samples were collected with the Nautile submersible (IFREMER) during the Flores mission in 1996 (Fouquet et al., 1998) and the Saldanha mission in 1998 (Barriga et al., 1998) and are identified with a FL and SAL

**Table 1**
Sediment and rock samples used in this study.

| | Sample | | Cruise/sampling method | Recovery (cm) | Depth (m) |
|---|---|---|---|---|---|
| Sediment cores | Away from the venting area | SH92 | Seahma'02/ROV "push-core" | 12 | 2125 |
| | | SCD8 | CD167, 2004/gravity core | 91 | 2300 |
| | Venting area | SH118T | Seahma'02/ROV "spade" | [a] | 2214 |
| | | SH119 | Seahma'02/ROV "push-core" | 12 | 2213 |
| | | SCD7 | CD167'04/gravity core | 27 | 2198 |
| | Sample | | Cruise/sampling method | Lithology | Depth (m) |
| Rock samples | SAL-06-08 (B1) | | Saldanha'98/Nautile | Fresh basalt | 2223 |
| | SAL-09-15 (B2) | | Saldanha'98/Nautile | Fresh basalt | 2421 |
| | FL-12-12 (MB1) | | Flores'96/Nautile | Metabasalt | 2217 |
| | FL-12-14 (MB2) | | Flores'96/Nautile | Metabasalt | 2232 |
| | SAL-06-09 (MG1) | | Saldanha'98/Nautile | Metagabbro | 2220 |
| | SAL-06-10 (MG2) | | Saldanha'98/Nautile | Metagabbro | 2205 |
| | FL-12-11 (Serp1) | | Flores'96/Nautile | Serpentinite | 2247 |
| | FL-06-06 (Serp2) | | Flores'96/Nautile | Serpentinite | 2225 |
| | SAL-10-01 (ST1) | | Saldanha'98/Nautile | Steatite | 2359 |
| | SAL-10-04 (ST2) | | Saldanha'98/Nautile | Steatite | 2285 |

[a] The first layers of the sediment were mixed during recovery.

prefix, respectively. For each lithology identified during these cruises, two representative rock samples were selected for analysis according to petrographic and geochemical features described in preliminary studies (Costa, 2001; Ribeiro da Costa, 2005) (Table 1). The location of the sediment and rock samples used in this study is shown in Fig. 1.

Rare earth elements (REE) analyses for the Fe–Mn crust of the SH118T sediment core and from rock samples were carried out at "Activation Laboratories, Ltd" (Actlabs, Ontário, Canada), following standard procedures. Before analyses, samples were carefully powdered in agate mortar and REE were determined by Inductively Coupled Plasma Mass Spectrometry after a lithium metaborate–tetraborate fusion. Measured accuracy was better than 5%. REE data for sediments, with the exception of the Fe–Mn crust, are from Dias et al. (submitted for publication) which used the same method.

Lead and Nd isotopes were measured at the National Oceanography Centre, Southampton (NOCS), the Pb isotopes on a VG Sector 54 Thermal Ionisation Mass Spectrometer and Nd using a Thermo Neptune Multi Collector – Inductively Coupled Plasma – Mass Spectrometry (MC–ICP–MS).

After drying, the sediment and rock samples were carefully crushed in an agate mortar and pestle and fully digested using a four-step procedure: (1) 6 M HCl; (2) a mixture of 3 ml HCl and 1 ml $HNO_3$; (3) 3 ml HF and; (4) 1.5 ml HBr. At the end of each digestion step the samples were dried on a hotplate.

The samples were prepared for the mass spectrometer using standard ion exchange chemistry. Pb was isolated using AG1-X8 200–400 mesh anion exchange resin in a two column procedure. Procedural blanks were <50 pg, which is negligible relative to the amount of Pb recovered. Measurements were made using a Pb double spike procedure with the Southampton-Brest-Lead 207-204 spike (SBL74). Both natural and spiked runs were measured using a dynamic routine modified after Thirlwall (2000). Natural run ion beam intensities of $^{208}Pb$ were all $>1\times10^{-11}$ A. NBS SRM-981 measurements made over a 5 year period gave the average ratios: $^{206}Pb/^{204}Pb = 16.9403 \pm 32$, $^{207}Pb/^{204}Pb = 15.4980 \pm 32$, $^{208}Pb/^{204}Pb = 36.7225 \pm 85$ ($n = 112$, $\pm 2$ S.D. in the last quoted figures).

The waste from the Pb columns was dried down and used for the Nd analyses. The Nd procedure uses a AG50 cation resin column to separate the REE from the matrix followed by a Ln-Spec column to isolate the Nd from the other REE. The measurements were carried out on the Neptune MC–ICP–MS using static collection mode on 7 faraday detectors, producing an average of 150 ratios. Isotope ratios were corrected for mass bias by normalization to $^{146}Nd/^{144}Nd = 0.7219$. Measured values for JNdi-1 were $^{143}Nd/^{144}Nd = 0.512082 \pm 14$ (2 S.D., $n = 8$) during the measurement period, and are corrected to $^{143}Nd/^{144}Nd = 0.512115$ (Tanaka et al., 2000). The $\varepsilon_{Nd(0)}$ values were determined by comparison to the Chondrite Uniform Reservoir (CHUR) for the present day, where $(^{143}Nd/^{144}Nd)_{CHUR} = 0.512638$ (DePaolo and Wasserburg, 1976).

## 3. Brief sample description

Saldanha sediments comprise three dominant components: (1) biogenic and pelagic input from the upper water column; (2) locally-derived detrital material from the outcropping basement; and (3) minerals precipitated from hydrothermal fluids (Dias and Barriga, 2006). With the exception of core SCD7, all other sites are dominated by pelagic foraminiferal oozes with minor locally-derived detrital components. The SH119 and SH118T samples, collected from active vent orifices, show minor hydrothermal alteration, characterized by Mn and Fe oxyhydroxides phases with occasional millimetre sized grains of chalcopyrite, sphalerite and pyrite; lithoclasts in these cores are dominated by altered ultramafic rocks (serpentinites and steatites). In the two sediment cores collected away from the venting area (SH92 and SCD8), sulphide minerals were not identified and lithoclasts are mostly altered mafic rocks.

Core SCD7, collected from an area of active venting, contains many fragments of millimetre to centimetre sized metabasalts and -gabbros in the upper 5 cm of the core. Below 5 cmbsf the sediment is dominated by hydrothermal minerals characterized by chalcopyrite + sphalerite/wurtzite ± pyrite (filling veins and as millimetre sized grains disseminated in the sediment matrix) and millimetre to centimetre sized crystalline hydrothermal calcite. The sediment matrix is composed of serpentine + talc ± chlorite, with variable amounts of millimetre sized lithoclastic debris; usually comprising less than 5% in the upper layers and almost nonexistent below 7 cmbsf. Lithoclasts were identified as serpentinites, steatites and metagabros/metabasalts, most of them showing microdeformation texture. The biogenic/pelagic component occurs only in the upper part of this sediment core but in negligible proportions.

Basalt samples (B1 and B2) are pillow lavas with a porphyritic matrix with some olivine phenocrysts and containing vesicles up to 0.5 mm in diameter. Petrographic observations revealed that these samples are composed of plagioclase, olivine and pyroxene in a fine-grained matrix composed of glass, plagioclase, pyroxene and olivine. Metasomatized basalts (MB1 and MB2) exhibit a green and/or gray matrix due to intense chloritization and/or silicification of pillow lavas. Sample MB1 has a relict porphyritic texture whereas in sample MB2 the mineralogy and texture of the original lava is not observed. Chlorite and Mn-carbonates are pervasive in the matrix and are cut by silica veins. Some geodes composed of euhedral quartz crystals and oxidized sulphide minerals are present in sample MB2. This mineralogy and textures are consistent with intense chloritization and

silicification. Mass balance estimates for these samples (Costa, 2001) show enrichments in Si, S, Cu, Zn, Co, Mn, As, Br and $CO_2$ in sample MB2 compared with MB1, consistent with the observed mineralogy and indicative of sulphide mineralization and silicification.

Metasomatized gabbros were sampled in the northern part of the Saldanha massif in a NNE–SSW alignment. The two selected samples (MG1 and MG2) are deformed medium-grained metagabbros with some alteration and deformation of the primary igneous textures. Nevertheless, some primary igneous minerals (plagioclase and clinopyroxene) could be recognized defining a linear orientation (particularly evident in sample MG1). In these two samples, primary pyroxene show pervasively replacement by actinolite and chlorite and chlorite + epidotite + quartz filled veins and fractures. Primary and secondary mineral textures suggest deformation during and after metasomatic events.

Ultramafic rocks from the Saldanha massif (usually harzburgites) are variably altered either to serpentinites or to steatites (talc-bearing serpentinites). The selected serpentinite samples (Serp1 and Serp2) are from chromite-free dunite. These completely serpentinized rocks have recrystallized mesh textures and minor amounts of orthopyroxene-bastites (in Serp1), with accessory magnetite (2–7%). The serpentine minerals are lizardite and chrysotile, in present variable proportions.

The two steatite samples consist of a completely steatized serpentinite (ST1: ~100% talc) and a partially steatized serpentinite (ST2: >75% talc). In ST2, talc predominantly pseudomorphs the mesh texture typical of the original serpentinite. Serpentinite replacement by talc is interpreted to result from Si-metasomatism, as consequence of interaction with reduced fluids with high silica contents that may have derived from fluid interaction with deep-seated gabbros (e.g. Bach et al., 2004; Bach and Klein, 2007, 2009). This interpretation is also supported by the very low $Al_2O_3/SiO_2$ ratios of these talc-rich rocks (ST1-$Al_2O_3/SiO_2$ = 0.008 and ST2-$Al_2O_3/SiO_2$ = 0.013; Costa, 2001).

## 4. Results

### 4.1. Rare earth elements

REE concentrations were normalized to chondrite values (Taylor and McLennan, 1985) and the deviations of Eu and Ce from the rest of REEs where defined by Eu and Ce anomalies ($Eu/Eu^* = (Eu/Eu_{CN})/[(Sm/Sm_{CN} + Gd/Gd_{CN})/2]$ and $Ce/Ce^* = (Ce/Ce_{CN})/[(La/La_{CN} + Pr/Pr_{CN})/2]$, respectively) and are presented in Table 2. Chondrite-normalized REE patterns are shown in Fig. 2.

The REE data for the Saldanha sediment cores are described in Dias et al. (submitted for publication) and are presented in Fig. 2a. The sediments exhibit two distinct REE patterns: (1) the majority of sediment cores show a similar pattern, characterized by a depletion in heavy REE (HREE), a negative Ce anomaly ($(Ce/Ce^*)_{CN}$ average = 0.60) and a slight negative Eu anomaly ($(Eu/Eu^*)_{CN}$ average = 0.77); (2) a distinctive REE pattern shown by the SCD7 sediment core. This core displays variable REE patterns with depth. Above 8 cmbsf a flat REE pattern with a pronounced negative Eu anomaly with enriched REE contents occurs, while between 16 and 21 cmbsf a positive Eu anomaly with light REE (LREE) enrichment is observed. Below 22 cmbsf the pattern is similar to that of the upper layers, although with lower REE contents. The REE patterns for intermediate layers (8–16 cmbsf) are consistent with mixing between the upper core and the deeper material. The Fe–Mn crust exhibits a different pattern compared with the sediment cores, including the sediment below the cap (SH118T), displaying enrichment in LREE and no negative Ce anomaly (Fig. 2a).

The two basalt samples have similar chondrite-normalized REE patterns, characterized by relatively flat patterns, around ten times chondrite, with a slight LREE enrichment (Fig. 2b). One of the metabasalt samples (MB1) has a flat REE pattern similar to fresh basalts, whereas, the other metabasalt sample (MB2) and the metagabbros (MG1 and MG2) show a slight depletion in REE contents, and a positive Eu anomaly. Altered ultramafic samples (serpentinites and steatites) are extremely REE-depleted relative to chondrite, with some REE being below the analytical detection limit (Fig. 2b). They display a U-shaped pattern as a consequence of their relative enrichment in LREE and HREE, compared to the intermediate REE (Table 2 and Fig. 2b). These rocks show positive Eu anomalies, ranging from 1.31 to 8.00 (the highest value corresponding to the ST2 steatite), and more uniform Ce anomalies, ranging between 0.53 and 0.77.

### 4.2. Neodymium isotopes

The $^{143}Nd/^{144}Nd$ isotope ratios and $\varepsilon_{Nd(0)}$ values determined for the Saldanha rocks and sediments are listed in Table 3. $\varepsilon_{Nd(0)}$ values are plotted in Fig. 3, together with data for N-Famous and AMAR-S basalt rocks (Dosso et al., 1999), TAG hydrothermal sediments and ferromanganese crusts (Mills et al., 1993, 2001) and Lucky Strike hydrothermal sediments (Dias et al., 2008) for comparison. Reference values for North Atlantic Deep Water (NADW, Piepgras and Jacobsen, 1992) and mantle peridotite (Workman and Hart, 2005) are also plotted and considered as end-members to estimate the relative contribution of these sources in the samples.

$^{143}Nd/^{144}Nd$ isotope ratios in Saldanha sediment cores fall into two distinct groups. SCD7 displays the most radiogenic values ranging from 0.513049 to 0.513170 ($\varepsilon_{Nd(0)} = +8.01$ to $+10.37$), while the remaining samples exhibit non-radiogenic Nd isotopic ratios ranging from 0.512098 to 0.512236 ($\varepsilon_{Nd(0)} = -10.53$ to $-7.85$). The higher value of this latter group of samples corresponds to the Fe–Mn crust (SH118T).

All mafic rock samples (both fresh and altered) exhibit a narrow range of $^{143}Nd/^{144}Nd$ ratio values between 0.513076 and 0.513156 ($\varepsilon_{Nd(0)} = +8.57$ to $+10.11$). Altered ultramafic rock samples (serpentinites and steatites) have much lower ratios, ranging between 0.512625 and 0.512716 ($\varepsilon_{Nd(0)} = -0.25$ to $+1.52$).

### 4.3. Lead isotopes

The Pb isotope ratios of the Saldanha samples are listed in Table 3 and their distribution is plotted on conventional inter-isotopic ratio diagrams (Fig. 4). In order to identify the Pb sources, Pb isotope data are plotted together with reference values of (1) Northern Hemisphere Reference Line (NHRL: Hart, 1984); (2) North Atlantic Sediment Line (NASL), defined by Pb isotope ratios of pelagic, terrigenous and biogenic Atlantic sediments (Ben Othman et al., 1989) and; (3) Atlantic seawater inferred from hydrogenetic Fe–Mn crusts (von Blanckenburg et al., 1996). Data from other sites were also used for comparison.

Except for the SCD7 and SH118T sediment cores, Pb isotope ratios for sediment samples are fairly uniform: $^{206}Pb/^{204}Pb$ = 18.549–19.096, $^{207}Pb/^{204}Pb$ = 15.630–15.637 and $^{208}Pb/^{204}Pb$ = 38.501–39.163. The Pb isotope composition is relatively radiogenic and plots away from the NHRL, close to the NASL (Table 3 and Fig. 4a–b). Core SCD7 displays variable Pb isotopic ratios down core (Figs. 4 and 5): (1) at 7–8 cmbsf the Pb isotopic composition is more radiogenic than the NHRL, and is shifted away from the FAMOUS-AMAR values towards the two serpentinite samples; (2) at 11–13 cmbsf the Pb isotopic composition is relatively non-radiogenic, similar to hydrothermally altered samples (steatites, metabasalts and metagabbros), and plots with the FAMOUS-AMAR samples; (3) at 19–21 cmbsf the Pb isotopic ratios are much less radiogenic than local rocks, which is reflected in low $^{206}Pb/^{204}Pb$ (17.9473) and $^{208}Pb/^{204}Pb$ (37.7302) ratios; (4) the deepest layers (21–27 cmbsf) have the most radiogenic Pb composition which are close to seawater ratios and closer to the serpentinite isotopic composition. The Fe–Mn crust from sample SH118T exhibits distinct values from the remaining sediment of that core (Fig. 4a). Non-radiogenic values are observed in the sediment while radiogenic, seawater values, are recorded in the Fe–Mn crust.

**Table 2**
REE composition from Saldanha rock and sediment samples. Values for marine sediments, Rainbow hydrothermal fluids and seawater are also included.

| | | | La | Ce | Pr | Nd | Sm | Eu | Gd | Tb | Dy | Ho | Er | Tm | Yb | Lu | $(La/Sm)_{CN}$ | $(Gd/Yb)_{CN}$ | $(La/Yb)_{CN}$ | Ce/Ce* | Eu/Eu* |
|---|---|---|---|---|---|---|---|---|---|---|---|---|---|---|---|---|---|---|---|---|---|
| Sediment core samples | SCD7[a] | <5 cmbsf | 3.44 | 8.11 | 1.24 | 6.55 | 1.94 | 0.52 | 2.47 | 0.50 | 3.22 | 0.69 | 2.14 | 0.33 | 2.09 | 0.31 | 1.12 | 0.96 | 1.11 | 0.92 | 0.72 |
| | | 5–7 cmbsf | 3.81 | 8.78 | 1.37 | 7.14 | 2.05 | 0.50 | 2.75 | 0.53 | 3.37 | 0.70 | 2.16 | 0.33 | 2.12 | 0.31 | 1.17 | 1.05 | 1.21 | 0.90 | 0.64 |
| | | 7–8 cmbsf | 2.56 | 6.80 | 1.14 | 5.95 | 1.91 | 0.45 | 2.40 | 0.49 | 3.27 | 0.67 | 2.02 | 0.30 | 1.89 | 0.28 | 0.84 | 1.03 | 0.92 | 0.93 | 0.64 |
| | | 9–10 cmbsf | 1.75 | 4.40 | 0.74 | 3.61 | 1.04 | 0.32 | 1.41 | 0.27 | 1.77 | 0.39 | 1.19 | 0.18 | 1.17 | 0.18 | 1.06 | 0.98 | 1.01 | 0.90 | 0.82 |
| | | 11–13 cmbsf | 1.57 | 4.00 | 0.66 | 3.30 | 0.99 | 0.34 | 1.28 | 0.25 | 1.67 | 0.36 | 1.07 | 0.16 | 1.01 | 0.16 | 1.00 | 1.03 | 1.05 | 0.92 | 0.91 |
| | | 13–16 cmbsf | 2.02 | 4.06 | 0.51 | 2.32 | 0.60 | 0.24 | 0.82 | 0.17 | 1.10 | 0.23 | 0.67 | 0.10 | 0.64 | 0.10 | 2.12 | 1.04 | 2.13 | 0.92 | 1.05 |
| | | 16–17 cmbsf | 0.84 | 1.70 | 0.25 | 1.27 | 0.33 | 0.16 | 0.43 | 0.07 | 0.47 | 0.10 | 0.31 | 0.05 | 0.29 | 0.05 | 1.60 | 1.20 | 1.96 | 0.86 | 1.30 |
| | | 17–19 cmbsf | 1.19 | 2.29 | 0.30 | 1.39 | 0.37 | 0.18 | 0.49 | 0.08 | 0.46 | 0.09 | 0.28 | 0.04 | 0.26 | 0.04 | 2.02 | 1.53 | 3.09 | 0.88 | 1.29 |
| | | 19–21 cmbsf | 1.12 | 1.80 | 0.27 | 1.29 | 0.38 | 0.20 | 0.35 | 0.06 | 0.35 | 0.07 | 0.21 | 0.03 | 0.16 | 0.02 | 1.86 | 1.77 | 4.73 | 0.75 | 1.68 |
| | | 22–23 cmbsf | 1.15 | 2.27 | 0.30 | 1.52 | 0.47 | 0.12 | 0.55 | 0.10 | 0.69 | 0.15 | 0.46 | 0.07 | 0.46 | 0.07 | 1.54 | 0.97 | 1.69 | 0.89 | 0.74 |
| | | 25–27 cmbsf | 2.19 | 4.54 | 0.66 | 2.99 | 0.80 | 0.20 | 1.02 | 0.17 | 1.02 | 0.22 | 0.64 | 0.09 | 0.60 | 0.10 | 1.73 | 1.39 | 2.48 | 0.88 | 0.66 |
| | | Mean | 1.97 | 4.43 | 0.68 | 3.39 | 0.99 | 0.29 | 1.27 | 0.24 | 1.58 | 0.33 | 1.01 | 0.15 | 0.97 | 0.15 | 1.73 | 1.39 | 2.48 | 0.89 | 0.66 |
| | SH92[a] | Mean | 8.20 | 10.45 | 1.84 | 6.65 | 1.48 | 0.39 | 1.60 | 0.27 | 1.61 | 0.33 | 0.97 | 0.14 | 0.81 | 0.12 | 3.50 | 1.61 | 7.19 | 0.61 | 0.77 |
| | SH119[a] | Mean | 6.76 | 9.37 | 1.67 | 6.12 | 1.41 | 0.35 | 1.36 | 0.22 | 1.30 | 0.26 | 0.73 | 0.10 | 0.61 | 0.09 | 3.03 | 1.81 | 8.12 | 0.64 | 0.76 |
| | SH118T[a] | Mean | 7.21 | 9.10 | 1.77 | 6.18 | 1.42 | 0.37 | 1.38 | 0.23 | 1.43 | 0.29 | 0.85 | 0.12 | 0.70 | 0.10 | 3.20 | 1.60 | 7.48 | 0.58 | 0.81 |
| | SH118 | CRUST | 5.50 | 11.00 | 1.26 | 4.51 | 0.94 | 0.20 | 0.74 | 0.12 | 0.71 | 0.15 | 0.47 | 0.07 | 0.45 | 0.07 | 3.68 | 1.33 | 8.26 | 0.95 | 0.75 |
| | SCD8[a] | mean | 9.29 | 12.03 | 2.30 | 8.25 | 1.78 | 0.47 | 1.87 | 0.31 | 1.81 | 0.36 | 1.03 | 0.15 | 0.85 | 0.12 | 3.20 | 1.60 | 7.48 | 0.58 | 0.81 |
| Rock samples | B1 | SAL-06-08 | 4.39 | 10.00 | 1.42 | 6.49 | 2.00 | 0.75 | 2.43 | 0.43 | 2.98 | 0.63 | 1.76 | 0.29 | 1.83 | 0.29 | 1.38 | 1.08 | 1.62 | 0.94 | 1.04 |
| | B2 | SAL-09-15 | 5.98 | 13.00 | 1.89 | 8.65 | 2.46 | 0.92 | 2.97 | 0.55 | 3.43 | 0.73 | 2.15 | 0.34 | 2.09 | 0.32 | 1.53 | 1.15 | 1.93 | 0.90 | 1.04 |
| | MB1 | FL-12-12 | 3.98 | 10.00 | 1.52 | 7.54 | 2.57 | 0.98 | 3.11 | 0.61 | 4.16 | 0.86 | 2.36 | 0.41 | 2.56 | 0.35 | 0.97 | 0.98 | 1.05 | 0.95 | 1.06 |
| | MB2 | FL-12-14 | 1.55 | 3.70 | 0.59 | 3.10 | 1.11 | 0.63 | 1.59 | 0.29 | 1.95 | 0.41 | 1.22 | 0.20 | 1.18 | 0.20 | 0.88 | 1.09 | 0.89 | 0.91 | 1.45 |
| | MG1 | SAL-06-09 | 2.17 | 4.70 | 0.66 | 3.14 | 0.98 | 0.50 | 1.12 | 0.20 | 1.31 | 0.27 | 0.76 | 0.13 | 0.81 | 0.13 | 1.39 | 1.12 | 1.81 | 0.92 | 1.45 |
| | MG2 | SAL-06-10 | 1.49 | 3.30 | 0.50 | 2.43 | 0.77 | 0.38 | 0.98 | 0.19 | 1.23 | 0.25 | 0.72 | 0.13 | 0.63 | 0.11 | 1.22 | 1.26 | 1.60 | 0.89 | 1.33 |
| | Serp1 | FL-12-11 | 0.19 | 0.20 | 0.02 | 0.10 | 0.02 | 0.01 | 0.03 | <0.01 | 0.02 | <0.01 | 0.02 | 0.01 | 0.05 | 0.02 | 5.98 | 0.49 | 2.57 | 0.63 | 1.37 |
| | Serp2 | Fl-06-06 | 0.28 | 0.30 | 0.04 | 0.13 | 0.03 | 0.01 | 0.03 | <0.01 | 0.04 | <0.01 | 0.03 | 0.01 | 0.05 | 0.01 | 5.87 | 0.49 | 3.78 | 0.59 | 1.31 |
| | ST1 | SAL-10-01 | 0.12 | 0.20 | 0.03 | 0.10 | 0.03 | 0.02 | 0.04 | <0.01 | 0.04 | <0.01 | 0.03 | 0.01 | 0.04 | 0.01 | 2.52 | 0.81 | 2.03 | 0.77 | 1.68 |
| | ST2 | SAL-10-04 | 0.18 | 0.20 | 0.04 | 0.22 | 0.03 | 0.10 | 0.05 | <0.01 | 0.06 | 0.01 | 0.04 | 0.01 | 0.05 | 0.01 | 3.78 | 0.81 | 2.43 | 0.53 | 8.00 |
| Marine sediments[b] | | | 26.10 | 55.20 | 7.34 | 30.00 | 5.59 | 1.60 | 6.33 | 1.04 | 0.61 | 1.03 | 3.08 | 0.47 | 3.03 | | 2.94 | 1.69 | 5.81 | 0.93 | 0.82 |
| Rainbow $10^3$[c] | | | 16.67 | 8.35 | 0.52 | 1.59 | 0.30 | 4.68 | 0.46 | 0.05 | 0.28 | 0.05 | 0.12 | | 0.06 | 0.01 | 34.88 | 6.47 | 197.26 | 0.35 | 38.53 |
| SW $10^4$ (1500–2500 depth)[d] | | | 2.61 | 1.79 | | 2.20 | 0.42 | 0.09 | 0.63 | | | | 0.52 | | 0.49 | | 3.88 | 1.04 | 3.61 | 0.53 | 0.55 |

CN: chondrite normalization.
[a] Dias et al. (unpublished).
[b] Wildeman and Haskin (1965).
[c] Douville et al. (2002).
[d] Elderfield and Greaves (1982).

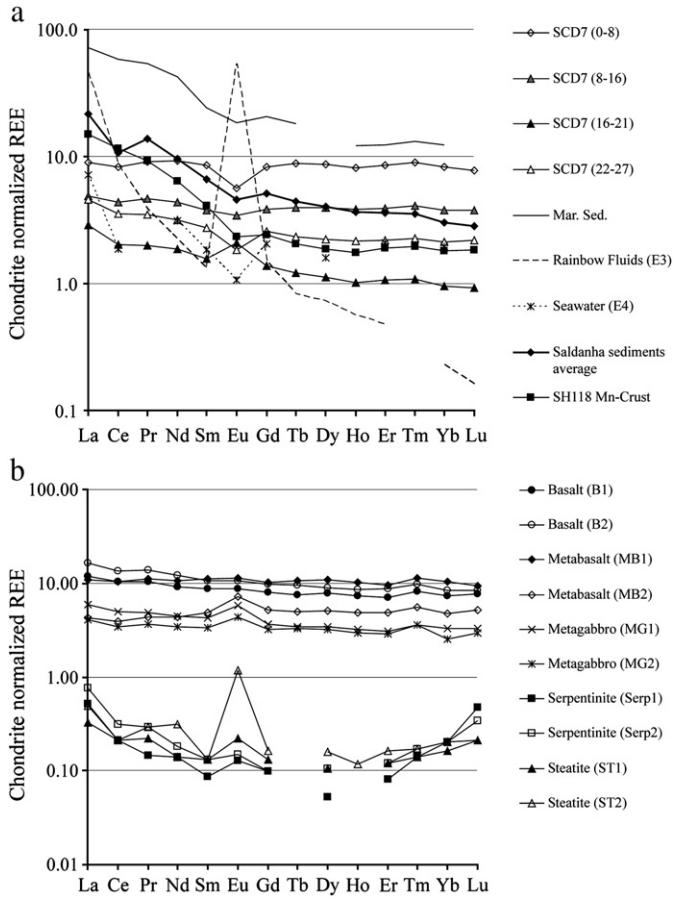


**Fig. 2.** Chondrite-normalized REE patterns from Saldanha (a) sediments and the Fe–Mn crust, and; (b) rocks. Data for sediments are from Dias et al. (unpublished); for marine sediments from Wildeman and Haskin (1965); for Rainbow hydrothermal fluids ($\times 10^3$) from Douville et al. (2002); and for seawater ($\times 10^4$; 1500–2500 m depth) from Elderfield and Greaves (1982).

All mafic rocks (fresh and altered) display non-radiogenic Pb isotopic values, plotting on or close to the NHRL and falling within the range for the FAMOUS-AMAR segment (Dosso et al., 1999). Only one basalt sample (B2) exhibits a somewhat higher $^{207}Pb/^{204}Pb$ ratio, deviating from other local mafic rocks and from the NHRL and FAMOUS-AMAR mafic rocks towards seawater values (Fig. 4c–d). The most radiogenic Pb ratios were found in serpentinites. The two studied samples, however, do not display homogeneous values. Serp1 displays more radiogenic Pb values than Serp2. Steatites, on the other hand, have non-radiogenic Pb values, similar to the mafic rock values.

## 5. Discussion

### 5.1. REE and Nd isotope composition

Chondrite-normalized REE patterns for pelagic ooze dominated samples SH92, SH118T, SH119 and SCD8 are comparable with normal pelagic sediments (e.g. Wildeman and Haskin, 1965). The negative Ce anomalies and non-radiogenic Nd compositions, which plot close to the NADW composition (Piepgras and Jacobsen, 1992), imply that significant REE scavenging from seawater has occurred, probably by Fe–Mn oxyhydroxide phases. More radiogenic $\varepsilon_{Nd(0)}$ values were observed in some layers of these cores, suggesting enhanced Nd contribution from hydrothermal sources. Similar $\varepsilon_{Nd(0)}$ values have been reported for plume derived sediments from the TAG hydrothermal field and this was interpreted of hydrothermal and seawater Nd in the vicinity of active venting (Mills et al., 1993; Godfrey et al., 1994).

In the Fe–Mn crust of sample SH118T, the LREE enrichments together with the lack of a negative Ce anomaly and high $\varepsilon_{Nd(o)}$ values (−7.85), suggest that this crust is not hydrogenetic in origin. Hydrogenetic ferromanganese crusts have positive Ce anomalies and Nd isotopic compositions similar to seawater as a consequence of REE uptake from seawater during their formation (e.g. Goldberg et al., 1963; Elderfield and Greaves, 1981; German, 1998). The LREE enrichment observed here indicates a hydrothermal fluid contribution during crust formation. The fact that the crust REE pattern does not have a positive Eu anomaly could be related to the low-temperature of the hydrothermal fluid or a significant seawater uptake overprinting the hydrothermal REE pattern. Previous mineralogical studies of this Fe–Mn crust also suggested a hydrothermal contribution in their genesis, based on the dominant todorokite mineralogy and chemistry (Dias et al., 2005). Moreover, the REE and Nd isotopic content recorded in this Fe–Mn crust fall in the range of the TAG hydrothermal ferromanganese crusts (Mills et al., 2001).

The SCD7 core has variable REE content. LREE enrichment and positive Eu anomalies, particularly evident between 16 and 21 cmbsf, are a consequence of sulphide minerals precipitation from hydrothermal fluids (e.g. Mills and Elderfield, 1995; German et al., 1999). In the other layers of this core, REE patterns have both negative and positive Eu anomalies and variable REE content, as a consequence of the different amounts of talc and serpentinite present and variation in the detrital component. In the upper core (<8 cmbsf) Nd concentrations are nine times that of chondrite and this is consistent with the major amounts of lithoclasts found in this part of the sediment Dias et al. (submitted for publication) that contribute higher REE contents than hydrothermal minerals which characteristically have low REE content.

The radiogenic Nd values from SCD7 ($\varepsilon_{Nd(0)} = +8.01$ to $+10.37$) are inferred to result from mineral precipitation from hydrothermal fluids that interacted with Saldanha mafic rocks at high temperatures, as they are similar to those recorded in mafic rocks from this region ($\varepsilon_{Nd(0)} = +8.57$ to $+10.11$). When compared with the TAG and Lucky Strike Nd isotopic signatures, SCD7 samples plot closer to Lucky Strike (Fig. 3). Lucky Strike sediments are more radiogenic than those from TAG, and are dominated by a hydrothermal fraction directly precipitated from hydrothermal fluids circulating through the underlying rocks, with minor seawater interaction (Dias et al., 2008). In contrast, TAG sediments show evidence for mass-wasting of sulphide material and dilution with the background pelagic sediment (Mills et al., 1993; Godfrey et al., 1994), resulting in lower Nd isotopic ratios. This is consistent with the non-pelagic content of core SCD7 and with a minor Nd isotopic contribution from seawater.

The REE composition of the Saldanha basalts ($(La/Sm)_{CH} = 1.38$ and 1.53) falls within the range for the transitional-mid-ocean ridges basalts (T-MORB) from the Azores southern ridge ($1.8 > (La/Sm)_{CH} > 0.7$; Schilling, 1975; Langmuir et al., 1977; Schilling et al., 1983). Basalt geochemical analyses in the MAR sector between the Azores platform (40°N) and 33° 30′N (Schilling, 1975; Dosso et al., 1999) have revealed heterogeneities along this ridge segment. The REE variation with latitude can be divided into two main groups: (1) the 40°N to 33.30°N sector, which includes the Saldanha site, is marked by a smooth and progressive northwest enrichment of LREE with a consequent increase of $(La/Sm)_{CH}$ ratios, which can be as high as 2–3 near the Azores islands; (2) south of 34°N, basalt patterns are characterized by LREE-depletion with $(La/Sm)_{CH}$ ratios lower than 1, typical of normal-mid-ocean ridge basalts (N-MORB). Basalts from the FAMOUS region (36° 47′N, MAR) have been characterized as basalts from a "transitional zone" (Schilling, 1975; Langmuir et al., 1977; Schilling et al., 1983) where both N-MORB, containing slight LREE-depletion characteristic of mid-ocean ridges ($(La/Sm)_{CN} \sim 0.62$), and LREE-enriched T-MORB ($(La/Sm)_{CN} \sim 1.3$ to 1.9) have been found, the latter being related to the Azores hot spot geochemical influence. Basalts collected in the studied area have LREE enrichments, though their $(La/Sm)_{CN}$ ratios are not as high as those

**Table 3**
Nd and Pb isotope composition of the Saldanha sediment and rock samples.

| | | | $^{143}Nd/^{144}Nd$ ±0.000015 | $\varepsilon_{Nd(0)}$ | $^{206}Pb/^{204}Pb$ | ± | $^{207}Pb/^{204}Pb$ | ± | $^{208}Pb/^{204}Pb$ | ± |
|---|---|---|---|---|---|---|---|---|---|---|
| Sediment samples | SCD7 | SCD7 (7–8) | 0.513137 | 9.74 | 18.763 | 0.006 | 15.622 | 0.005 | 38.614 | 0.013 |
| | | SCD7 (9–10) | 0.513170 | 10.37 | | | | | | |
| | | SCD7 (11–13) | 0.513155 | 10.09 | 18.803 | 0.004 | 15.564 | 0.003 | 38.407 | 0.009 |
| | | SCD7 (16–17) | 0.513088 | 8.77 | | | | | | |
| | | SCD7 (19–21) | 0.513049 | 8.01 | 17.947 | 0.004 | 15.559 | 0.004 | 37.730 | 0.008 |
| | | SCD7 (21–22) | 0.513126 | 9.52 | 19.100 | 0.004 | 15.669 | 0.003 | 39.142 | 0.009 |
| | | SCD7 (25–27) | 0.513135 | 9.70 | 18.691 | 0.003 | 15.645 | 0.003 | 38.656 | 0.008 |
| | SH92 | S92 (2–3) | | | 18.742 | 0.003 | 15.641 | 0.002 | 38.694 | 0.006 |
| | | S92 (6–7) | 0.512159 | −9.33 | 18.978 | 0.004 | 15.650 | 0.004 | 38.976 | 0.009 |
| | | S92 (10–11) | 0.512112 | −10.27 | 18.549 | 0.003 | 15.630 | 0.002 | 38.501 | 0.007 |
| | SH119 | S119 (2–3) | | | 18.999 | 0.003 | 15.659 | 0.003 | 39.025 | 0.007 |
| | | S119 (6–7) | 0.512129 | −9.93 | 18.816 | 0.008 | 15.642 | 0.006 | 38.806 | 0.016 |
| | | S119 (8–10) | 0.512147 | −9.57 | 18.993 | 0.004 | 15.662 | 0.003 | 39.021 | 0.008 |
| | SCD8 | SCD8 (0–2) | 0.512146 | −9.61 | 18.810 | 0.004 | 15.654 | 0.004 | 38.841 | 0.010 |
| | | SCD8 (4–6) | 0.512140 | −9.71 | 18.953 | 0.004 | 15.666 | 0.004 | 39.000 | 0.010 |
| | | SCD8 (8–10) | 0.512123 | −10.04 | 18.956 | 0.007 | 15.669 | 0.006 | 39.000 | 0.015 |
| | | SCD8 (12–14) | 0.512123 | −10.04 | 18.959 | 0.004 | 15.665 | 0.003 | 38.993 | 0.008 |
| | | SCD8 (20–22) | 0.512101 | −10.47 | | | | | | |
| | | SCD8 (40–42) | 0.512098 | −10.53 | 19.096 | 0.005 | 15.673 | 0.004 | 39.163 | 0.011 |
| | SH118 | total | 0.512148 | −9.55 | 18.649 | 0.010 | 15.559 | 0.008 | 38.314 | 0.020 |
| | | Crust | 0.512236 | −7.85 | 18.784 | 0.003 | 15.649 | 0.003 | 38.770 | 0.008 |
| Rock samples | B1 | SAL-06-08 | 0.513109 | 9.21 | 18.674 | 0.002 | 15.562 | 0.001 | 38.354 | 0.004 |
| | B2 | SAL-09-15 | 0.513110 | 9.19 | 18.597 | 0.004 | 15.590 | 0.004 | 38.342 | 0.012 |
| | MB1 | FL-12-12 | 0.513156 | 9.85 | 18.731 | 0.002 | 15.536 | 0.001 | 38.348 | 0.004 |
| | MB2 | FL-12-14 | 0.513143 | 10.10 | 18.865 | 0.004 | 15.548 | 0.003 | 38.458 | 0.010 |
| | MG1 | SAL-06-09 | 0.513076 | 9.97 | 18.906 | 0.003 | 15.548 | 0.003 | 38.486 | 0.009 |
| | MG2 | SAL-06-10 | 0.513149 | 8.54 | 18.626 | 0.007 | 15.527 | 0.007 | 38.242 | 0.021 |
| | Serp1 | FL-12-11 | 0.512708 | 1.37 | 18.673 | 0.045 | 15.646 | 0.045 | 38.498 | 0.125 |
| | Serp2 | FL-06-06 | 0.512716 | 1.52 | 18.922 | 0.005 | 15.593 | 0.005 | 38.666 | 0.015 |
| | ST1 | SAL-10-01 | 0.512625 | −0.25 | 18.891 | 0.003 | 15.544 | 0.003 | 38.470 | 0.009 |
| | ST2 | SAL-10-04 | 0.512716 | 1.52 | 18.842 | 0.001 | 15.545 | 0.001 | 38.435 | 0.004 |

reported for basalts collected nearer the Azores platform. Saldanha basalts previously studied by Costa (2001) display similar $(La/Sm)_{CN}$ values, but one of these samples has a much lower $(La/Sm)_{CN}$ ratio (0.6), falling in the range of N-MORB. Thus, the Saldanha site lies in the "transitional zone" under the influence of two distinct mantle sources; the Azores plume influence is only minor.

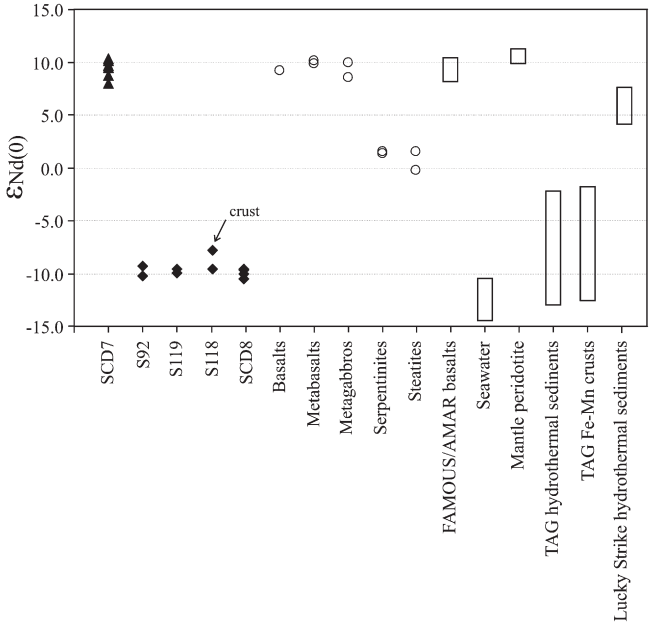


**Fig. 3.** $\varepsilon_{Nd(0)}$ values from Saldanha sediment and rock samples. $\varepsilon_{Nd(0)}$ values for N-Famous and AMAR-S rock samples (Dosso et al., 1999), modern seawater values (Piepgras and Jacobsen, 1992), TAG hydrothermal sediments and ferromanganese crusts (Mills et al., 1993, 2001) and Lucky Strike hydrothermal sediments (Dias et al., 2008) are also plotted.

The REE pattern for a metabasalt sample (MB1) is similar to those for fresh basalts suggesting that the REE distribution is not affected by alteration in this sample. The mineralogy and geochemistry of this sample suggest limited fluid interaction with low water/rock ratios (Costa, 2001). The second metabasalt sample (MB2) and metagabbros (MG1 and MG2) show a slight REE-depletion, positive Eu anomaly ($(Eu/Eu^*)_{CN} = 1.33$ to 1.45) and lack a Ce anomaly, suggesting that REE mobility is controlled by a high temperature, more reducing fluid with a lower pH than seawater (Sverjensky, 1984; Michard, 1989; Klinkhammer et al., 1994; Allen and Seyfried, 2005). The larger Eu anomalies in samples MB2 and MG1 confirm petrographic observations which showed that these two samples present a higher degree of hydrothermal alteration.

There are no previously published isotopic data from the Saldanha region. The nearest rocks with known isotopic signatures are basalts from N-Famous and AMAR-S, north and south of the Saldanha area, respectively (Dosso et al., 1999). These mafic rocks have Nd isotopic compositions similar to the Saldanha data reported here. Saldanha metabasalts and metagabbros analysed in this study yield Nd isotopic composition similar to basalts ($\varepsilon_{Nd(0)} = +8.54$ to $+10.10$), and this is consistent with alteration by hydrothermal fluids ($\varepsilon_{Nd(0)} = \sim +10$) instead of seawater weathering, as interaction with seawater should modify the rock isotopic values towards seawater-like signatures (Fig. 3). Another possibility to explain the similar signatures of altered mafic rocks and basalts is that the Nd isotopic composition was not modified during hydrothermal alteration, as a result of low fluid/rock ratios. However, with higher-temperature fluids, isotopic modification might occur (Michard and Albarède, 1986; Snow and Dick, 1995). It is not possible to detect fluid signatures in those cases where the fluids have a similar Nd isotopic composition to the basalts and gabbros due to previous interaction with mafic rocks.

Serpentinites and steatites REE pattern are similar to those reported for depleted oceanic mantle that typically display a concave upward shape with a marked LREE and HREE enrichment relatively to non-

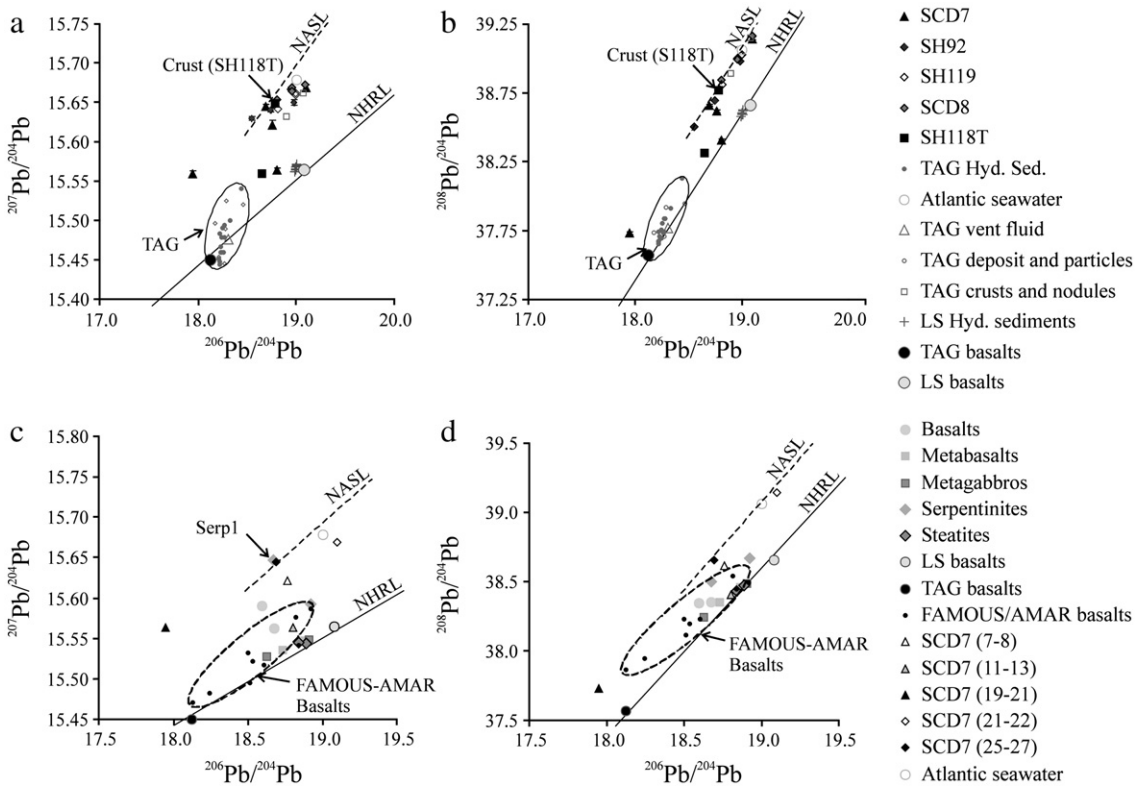


**Fig. 4.** Plots of $^{206}Pb/^{204}Pb$ versus $^{207}Pb/^{204}Pb$ and $^{206}Pb/^{204}Pb$ versus $^{208}Pb/^{204}Pb$ for Saldanha sediment samples (a and b) and core SCD7 and Saldanha rocks (c and d). Data from TAG hydrothermal sediments (German et al., 1993; Mills et al., 1993); TAG vent fluids, mound deposits, Fe–Mn nodules and crusts, plume particles and basalts (Godfrey et al., 1994); Lucky Strike hydrothermal sediments and basalts (Dosso et al., 1999; Ferreira, 2006; Dias et al., 2008); and basalts from Famous-Amar segments Langmuir et al., 1977) are also projected, as well as values for NHRL (Hart, 1984); NASL (Ben Othman et al., 1989) and Atlantic seawater (von Blanckenburg et al., 1996).

depleted mantle ultramafic rocks. High fluid fluxes are required to add enough REE to the rock and generate the LREE enrichment relative to the protolith. Similar U-shaped and LREE-enriched patterns have been described for dunites and harzburgites from, for example, Trinity ophiolite complex in California (Gruau et al., 1998) and Eastern Alps (Melcher et al., 2002).

It is generally accepted that LREE enrichments are not compatible with melting models for the upper mantle and it is thought that they are either a consequence of metasomatic processes, such as hydrothermal fluid alteration, or a refertilization by basaltic melts (Shaw, 1970; Prinzhofer and Allegre, 1985; McDonough and Frey, 1989; Sharma and Wasserburg, 1996; Savov et al., 2005). The REE pattern displayed by the Saldanha serpentinites seems to be the consequence of extensive seawater–peridotite interaction, and the positive Eu anomalies probably result from an interaction with reduced hydrothermal fluids. Other serpentinized peridotites such as those from MAR-15° 20′N (Paulick et al., 2006) and Mariana Forearc seamount (Savov et al., 2005) also exhibit LREE-enriched patterns and positive Eu anomalies, and these are interpreted to result from hydrothermal fluid–serpentinite interaction.

The REE patterns of steatites show, however, larger positive Eu anomalies relatively to serpentinites (especially sample ST2 with $Eu/Eu^* = 8.00$), which is consistent with more extensive reactions with

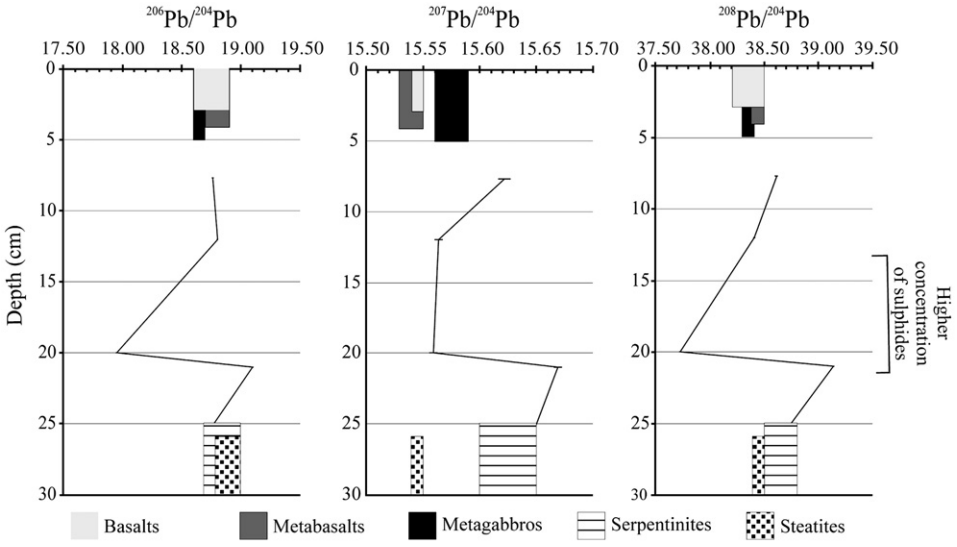


**Fig. 5.** SCD7 Pb isotope ratios down core. Range of Pb isotopic ratios from the different Saldanha lithologies are also represented.

reduced hydrothermal fluids, and a negative Ce anomaly resulting from seawater–rock interactions during precursor peridotite seawater alteration. Flat REE patterns with negative Eu anomalies have also been reported for talc samples from other MOR sites, e.g. talc-rich rocks from 15° 20′N MAR (Paulick et al., 2006) and even for some steatites from Saldanha and Rainbow sites (Costa, 2001; Marques et al., 2006 ). The REE signature of talc alteration from these sites deviates substantially from the signature of their serpentinized protolith, as these talc-rich rocks show negative Eu anomalies and a weak sloping or flat pattern. They also display an overall increased REE content, despite mass addition to the serpentinites, which could tend to dilute these elements. Eu anomalies in steatites are not well understood, it is thought that significant REE are added during talc alteration by silica-rich fluids. However, Eu does not follow this trend probably because it does not fit readily into the talc lattice. Nevertheless, steatites with positive Eu anomalies are observed at both the Saldanha and Rainbow sites (Costa, 2001; Marques et al., 2006 ) and in other oceanic environments (e.g. D'Orazio et al., 2004). In these cases, positive Eu anomalies are interpreted to be the result of hydrothermal alteration. In spite of some controversy concerning the Eu anomalies in talc-rich rocks, large positive Eu anomalies in steatites suggest a greater hydrothermal fluid influence than in serpentinites. These altered ultramafic rocks also show slightly negative Ce anomalies that have been recorded during the previously intense seawater–peridotite interaction (serpentinization process).

Saldanha serpentinites and steatites display $\varepsilon_{Nd(0)}$ close to zero ($\varepsilon_{Nd(0)} = -0.25$ to $+1.52$), falling between mantle peridotite and NADW compositions. The REE, and as a consequence the Nd isotopic composition of the oceanic crust, remain basically unchanged because they are essentially immobile except at high water/rock ratios and/or when rocks interact with high-temperature fluids (>350 °C, Michard and Albarède, 1986; Snow and Dick, 1995). Faure (1986) calculated that significant mobility of Nd takes place only at water/rock ratios over $10^5$ and that rock Nd isotopic ratios finally approach seawater values when this ratio reaches $10^8$. Thus, the low $\varepsilon_{Nd(0)}$ values of serpentinites and steatites most likely result from seawater–peridotite reaction at a high water/rock ratio.

The Nd isotopic composition and negative Ce anomalies recorded in steatites, similar to serpentinites, are likely to reflect the seawater–peridotite interaction that took place during the serpentinization process. The strong positive Eu anomaly observed in steatites, in particular in ST2 sample, but not in serpentinites, suggests a more pronounced interaction with high-temperature fluids after serpentinization.

### 5.2. Pb isotope composition

All sediments, with the exception of SCD7 and SH118T, have radiogenic Pb isotope compositions similar to the NASL, reflecting the significant pelagic component in these sediments which also dominates the REE and Nd isotopic composition.

In core SCD7, the less radiogenic Pb isotopic values occur between 7 and 21 cmbsf, and match those recorded in mafic rocks in the 11–13 cmbsf layer. Because rock fragments were rare below 7 cmbsf and the concentration of hydrothermal minerals is higher in this part of the core, this suggests an input of mafic-derived Pb from hydrothermal fluids. The radiogenic Pb composition between 19 and 21 cmbsf is lower than in local rocks or in any sample from the FAMOUS-AMAR segment. The large amount of sulphide minerals at this depth accounts for the less radiogenic values, although not for values lower than those measured in local rocks. Such low values might be due to measurement errors or to contamination during sample preparation or they may be a consequence of a less radiogenic source, such as hydrothermal fluids that have circulated through less enriched basalts or gabbros. Costa (2001) identified both N-MORBs and T-MORBs in the Saldanha area, which are sources of less radiogenic and more radiogenic Pb, respectively.

In the remaining sedimentary material of this core the Pb isotopic values are variable, with radiogenic values higher than the NHRL which plot away from the values reported for FAMOUS-AMAR area and for local rocks that do not exhibit seawater metasomatism. This variation is inferred to reflect the variable input of hydrothermal and detrital lithologenic material to this site. The serpentine, talc and minor chlorite observed in SCD7 contributes to the radiogenic values found throughout the core, which is reflected in the REE patterns (Fig. 2a).

In sample SCD7, a significant positive correlation between the Eu anomaly and Pb isotopic ratios is observed (Fig. 6), corroborating the hypothesis that non-radiogenic Pb values relate to hydrothermally-derived Pb (larger Eu anomaly).

A comparison of the less radiogenic Pb values from SCD7 with those from TAG and Lucky Strike sediments (Fig. 4a), indicates that the SCD7 sediment signatures are closer to the Lucky Strike sediment values and coincident with the more radiogenic values from TAG. The difference in the Pb isotopic signatures at these three sites is inferred to be a consequence of hydrothermal interaction with the different isotopic composition of the local basement rocks. The compositional difference in MAR basalts south of the Azores, between 34°N to 41°N, is well characterized (Schilling, 1975; Schilling et al., 1983; Dosso et al., 1999) and there is a gradual northwards enrichment in radiogenic Pb, associated with Azores mantle plume inputs. South of 34°N, this influence is not detected. The TAG hydrothermal field, located further south and outside the influence of the Azores plume, has less radiogenic sediments and basalts, whereas Lucky Strike (37°N) exhibits the highest radiogenic values because of the proximity of the Azores platform. The Saldanha area (36°N) has Pb isotope compositions similar to Lucky Strike values, which is consistent with the known Pb compositional variability along the MAR (Dosso et al., 1999). The same could be observed in relation to Nd isotopic composition where sediments from Lucky Strike show less radiogenic isotopic signatures relative to SCD7 because of the less radiogenic Nd values at those MAR latitudes (Dosso et al., 1999). Such differences give rise to fluids with different isotopic compositions, ultimately reflected in the sediments isotopic composition. In spite of the variability within core SCD7, the non-radiogenic Pb isotope ratios imply that hydrothermal fluids have reacted with mafic rocks rather than being serpentinization-derived fluids.

The Fe–Mn crust from sample SH118T contains radiogenic Pb and this is comparable to TAG Fe–Mn crusts, where this was interpreted to be the result of scavenging of Pb from seawater by the oxyhydroxides (Godfrey et al., 1994). In sediment from sample SH118T, collected below the crust cap, the non-radiogenic values suggest hydrothermal input into the pelagic sediment, and the higher ratios measured in the crust cap, near seawater compositions, are consistent with seawater Pb scavenging by the Mn oxyhydroxides overprinting any hydrothermal Pb contribution to the crust. This also suggests that the Fe–Mn crust acts as a barrier cap for the sediment below, minimizing seawater–sediment mixing processes and thus explaining the less radiogenic Pb signature derived from hydrothermal input.

Pb isotope values in the Saldanha basalts are consistent with previous values determined for rocks from that area of the MAR (Dosso et al., 1999), indicating a slight enrichment in more radiogenic Pb as a consequence of the Azores mantle plume influence, as described above. The non-radiogenic Pb isotope ratios displayed by the altered basalts and gabbros do not point to seawater interactions or, at least, seawater interactions were not sufficient to alter the isotopic composition of the rock, unlike the serpentinites. The mineralogy of the basalts indicates they have reacted with hydrothermal fluids that have reacted with mafic rock. However, the isotopic composition cannot be used to investigate this process as the fresh and metasomatised rocks have the same isotopic signature.

The more radiogenic Pb ratios of serpentinites result from extensive seawater reactions with the original peridotite, imprinting seawater Pb signatures on the rock. Variations of Pb isotopic ratios in the two

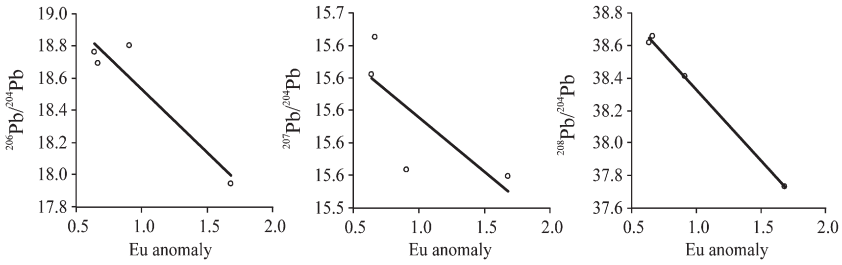


**Fig. 6.** Eu anomalies versus Pb isotope ratios in SCD7.

serpentinite samples analysed, especially in the $^{207}Pb/^{204}Pb$ ratio, could indicate either different amounts of seawater interaction during serpentinization, or late stage interaction of sample Serp2 with hydrothermal fluids that have circulated through mafic rocks. This latter interpretation is consistent with the observation of small positive Eu anomalies in Serp2 (Fig. 2).

In spite of the fact that Saldanha steatites have resulted from the replacement of serpentine by talc, they have non-radiogenic Pb values similar to the altered mafic rocks. This is the result of reactions of the precursor serpentinite with hydrothermal fluids that have circulated through mafic rocks, explaining not only the trend towards non-radiogenic Pb values, but also the increase in silica activity that promotes talc alteration. The introduction of silica to the system leads to an increase of sulphur fugacities that, in turn, promote sulphide precipitation (Klein and Bach, 2009), indicated by the presence of sulphide minerals in these samples.

### 5.3. Hydrothermal circulation at the Saldanha site

Chemical, isotopic and mineralogical evidence from this study indicates that the Saldanha field hydrothermal fluids encounter and react with diverse lithologies during fluid flow through fractured lithosphere. At the top of the Saldanha seamount, where the hydrothermal field is located, a heterogeneous melange of rock outcrops occur, including altered ultramafic and -gabbroic rocks. These lithologies have probably been tectonically emplaced at the seafloor by low-angle detachment faults, in similar way to other sites at NTOs along the MAR, including Saldanha (Gràcia et al., 2000). Ultramafic rocks show extensive serpentinization and this is the result of the deep faults occurring at this NTO that favour seawater penetration and serpentinization reactions with the upper mantle peridotite at depth (Gràcia et al., 2000; Mevel, 2003). Serpentinization is thought to induce a volumetric expansion (O'Hanley, 1992) and enhance crust permeability through faulting and fracturing which, in turn, further promotes fluid circulation The extensive presence of serpentinites implies the hydration of ultramafic rocks (Janecky and Seyfried, 1986; Berndt et al., 1996; Charlou et al., 2001; Holm and Charlou, 2001; Charlou et al., 2002; Allen and Seyfried, 2003) is the most plausible mechanism explaining the high $H_2$ and $CH_4$ anomalies detected in the seawater column overlaying the Saldanha field (Charlou et al., 1996; Bougault et al., 1998). $H_2$ may also be released during mafic–fluid reactions (Sugisaki et al., 1983; Wetzel and Shock, 2000), but in insufficient amounts to explain the large $H_2$ anomaly detected in the seawater column above Saldanha.

Serpentinization, however, cannot account for the hydrothermal alteration, silicification and sulphide precipitation, observed in steatites and metasomatized basalts and gabbros. Silica activity is low during the serpentinization process to increase this to allow for the silicification requires the fluids to react with mafic lithologies. The introduction of silica to the hydrothermal system also increases sulphur fugacities promoting sulphide precipitation. This suggests that fluids interact with mafic rocks, probably gabbroic intrusions, at depth, and along the fluid pathway react with serpentinites producing steatites, as proposed for example for the Kairei hydrothermal system (Nakamura et al., 2009). This is further corroborated by the low pH of the hydrothermal fluids, inferred from mineralogical and chemical signatures of hydrothermally altered samples, which is not typically associated with hydrothermal alteration processes in systems exclusively controlled by ultramafic rocks (Janecky and Seyfried, 1986; Berndt et al., 1996; Wetzel and Shock, 2000). Both silica and sulphur enrichments in Saldanha sediments and rocks can, therefore, be best explained by the involvement of gabbroic lithologies, common in Saldanha area. The higher temperature fluids responsible for the more intense hydrothermal alteration in Saldanha rocks and sediments are focused, reduced and enriched in Si and metals and acquire their Pb and Nd isotopic signatures during circulation not only through ultramafic but also through mafic rocks at depth.

Upflow of hydrothermal fluids takes place preferentially along highly permeable fracture zones and the fluids react with the host rocks, indicated by the occurrence of metabasalts, metagabbros and steatites mainly along the major NNE–SSW and NE–SW faults occurring at Saldanha area (Barriga et al., 2003; Miranda et al., 2003). These focused hydrothermal upflow zones also contain sediments with a more significant hydrothermal component, as observed in particular in the SCD7 sediment core. Despite these areas of more focussed venting, diffuse fluid venting through the sediment cover is the major venting style at this site.

## 6. Conclusions

Hydrothermal circulation in the Saldanha hydrothermal field is dominated by low-temperature diffuse fluid flow areas. The majority of Saldanha sediment samples are dominated by biogenic carbonate that masks the relatively minor hydrothermal Fe–Mn oxyhydroxide and sulphide phases. Consequently, the REE and Pb and Nd isotopic composition of most sediment samples are generally indistinguishable from pelagic sediments.

The exception to this is one sediment core (SCD7) that exhibits a distinctive geochemical signature and a more pronounced hydrothermal horizon at depth. The horizon in core SCD7 enriched in hydrothermal minerals has a Pb isotopic composition comparable to TAG and Lucky strike hydrothermal sediments. Cu–Zn sulphide precipitation and Pb and Nd isotopic composition in this core suggest that these elements are derived from high-temperature hydrothermal fluids that have reacted with mafic rocks.

Fresh basalts occur predominantly around the Saldanha seamount and exhibit transitional-MORB REE patterns which are similar to the more enriched basalts described for FAMOUS (Langmuir et al., 1977). The Saldanha basalt REE composition and Nd and Pb isotopic ratios are typical of MAR basalts and exhibit Azores mantle plume influence.

Serpentinized ultramafic rock outcrops mainly occur at the top and SW of the seamount and display REE patterns and isotopic compositions that arise from extensive seawater interactions with the peridotite protolith during serpentinization with minor evidences for interaction with hydrothermal fluids.

The hydrothermally altered basalts, gabbros and steatites are generally associated with the major faults identified in the area. Metagabbros and metabasalts show LREE enrichment with a positive Eu anomaly and non-radiogenic Pb and radiogenic Nd isotopic values

indicative of hydrothermal origin. Although steatites display negative Ce anomalies and Nd isotopic signatures similar to serpentinites, steatization (talc alteration) must have resulted from high silica activity implying a mafic-derived hydrothermal fluid, which also promoted sulphide mineralization in these rocks. A prominent positive Eu anomaly and Pb isotopic ratios similar to Saldanha mafic rocks are recorded in the steatites. Taken together, hydrothermal signatures in Saldanha altered rocks imply the interaction with high-temperature fluids that have encountered and reacted with gabbroic bodies along their pathway.

The data presented here show unequivocally that the Saldanha hydrothermal field is not simply a low-temperature and diffuse venting field driven by hydrothermal circulation through ultramafic rocks, as suggested previously (e.g. Barriga et al., 1998). Geochemical and isotopic evidence from sediments and rocks demonstrate that higher-temperature and more focused fluid flow also occurs at this site. Spatial variability in the fluid flow results in overprinted geochemical and isotopic signatures in rocks and sediments. The deeply penetrating faults appear to be preferential areas for the up flow of the high-temperature fluids that reacted with mafic rocks at depth. In spite of less intense hydrothermal venting at the Saldanha site than at other settings, the fluid up flow is focused in areas of fault enhanced permeability, minimizing seawater scavenging and oxidation processes within the sediment and rocks and promoting the hydrothermal mineralization.

## Acknowledgements

We thank all the participants in the Seahma's 2001 and CD167 cruises for various forms of indispensable cooperation in surveying and sampling. We are grateful to CREMINER's researchers and technicians and to NOCS Geochemistry staff for laboratory assistance. Financial support was provided by FCT (Portugal) through project SEAHMA (POCTI/MAR/15281/1999) and a PhD scholarship to the first author (SFRH/BD/8896/2002). We also thank the editor of Chemical Geology, Bernard Bourdon, and two anonymous reviewers for their helpful comments and suggestions.

## References

Allen, D.E., Seyfried Jr., W.E., 2003. Compositional controls on vent fluids from ultramafic-hosted hydrothermal systems at mid-ocean ridges: an experimental study at 400 °C, 500 bars. Geochimica et Cosmochimica Acta 67 (8), 1531–1542.

Allen, D.E., Seyfried Jr., W.E., 2004. Serpentinization and heat generation: constraints from Lost City and Rainbow hydrothermal systems. Geochimica et Cosmochimica Acta 68 (6), 1347–1354.

Allen, D.E., Seyfried Jr., W.E., 2005. REE controls in ultramafic hosted MOR hydrothermal systems: an experimental study at elevated temperature and pressure. Geochimica et Cosmochimica Acta 69 (3), 675–683.

Bach, W., Klein, F., 2007. Silica metasomatism of oceanic serpentinites. Geochimica et Cosmochimica Acta, 71, (15), Supplement 1, Goldschmidt Abstracts p. A48.

Bach, W., Klein, F., 2009. The petrology of seafloor rodingites: insights from geochemical reaction path modeling. Lithos 112 (1–2), 103–117.

Bach, W., Garrido, C.J., Paulick, H., Harvey, J., Rosner, M., 2004. Seawater–peridotite interactions: first insights from ODP Leg 209, MAR 15° N. Geochemistry Geophysics Geosystems 5 (9), Q09F26.

Barriga, F.J.A.S., et al., 1998. Discovery of the Saldanha hydrothermal field on the FAMOUS segment of the MAR (36° 30′N). Eos, Transactions, American Geophysical Union 79 (45), F67.

Barriga, F.J.A.S., et al., 2003. Seahma-1 Cruise Report Faculty of Sciences. University of Lisbon, Lisbon.

Ben Othman, D., White, W.M., Patchett, J., 1989. The geochemistry of marine sediments, island arc magma genesis, and crust–mantle recycling. Earth and Planetary Science Letters 94 (1–2), 1–21.

Berndt, M.E., Allen, D.E., Seyfried Jr., W.E., 1996. Reduction of $CO_2$ during serpentinization of olivine at 300 °C and 500 bar. Geology 24, 351–354.

Bougault, H., et al., 1998. FAMOUS and AMAR segment on the Mid-Atlantic Ridge: ubiquitous hydrothermal Mn, $CH_4$, $\delta^3$He signals along the rift valley walls and rift offsets. Earth and Planetary Science Letters 161, 1–17.

Cannat, M., et al., 1997. Ultramafic and gabbroic exposures at the Mid-Atlantic Ridge: geological mapping in the 15° N region. Tectonophysics 279 (1–4), 193–213.

Charlou, J.L., et al., 1993. Seawater $CH_4$ concentration over the Mid-Atlantic Ridge from the Hayes F.Z. to the Azores triple junction. Eos 74, 380.

Charlou, J.-L., et al., 1996. Methane degassing, hydrothermal activity and serpentinization between the Fifteen Twenty fracture zone area and the Azores Triple Junction area (Mid-Atlantic Ridge). The Journal of Conference Abstracts FARA-IR Mid-Atlantic Ridge Symposium, Reykjavik, Iceland, pp. 771–772.

Charlou, J.-L., et al., 1997. High methane flux between 15°N and the Azores Triple Junction, Mid-Atlantic ridge, hydrothermal and serpentinization processes. Eos, Transactions, American Geophysical Union 78 (F831).

Charlou, J.L., Donval, J., Fouquet, Y., Jean-Baptiste, P. and Holm, N.G., 2001. IRIS cruise results on the MAR (May 2001): hydrogen and organics from serpentinization, AGU Fall Meeting.

Charlou, J.-L., Donval, J.-P., Fouquet, Y., Jean-Baptiste, P., Holm, N.G., 2002. Geochemistry of high $H_2$ and $CH_4$ vent fluids issuing from ultramafic rocks at the Rainbow hydrothermal field (36°14′N, MAR). Chemical Geology 191, 345–359.

Costa, R., 2001. Estudo mineralógico e geoquímico da alteração hidrotermal das rochas vulcânicas e ultramáficas serpentinizadas do Monte Saldanha (RMA, Segmento FAMOUS /AMAR). MSc Thesis, Faculdade de Ciências da Universidade de Lisboa, Lisboa, 142 pp.

DePaolo, D.J., Wasserburg, G.J., 1976. Nd isotopic variations and petrogenetic models. Geophysical Research Letters 3 (5), 249–252.

Dias, A., Barriga, F., 2006. Mineralogy and geochemistry of hydrothermal sediments from the serpentinite-hosted Saldanha hydrothermal field (36°34′N; 33°26′W) at MAR. Marine Geology 225, 157–175.

Dias, A., Jorge, R.C.G.S., Barriga, F.J.A.S., 2005. Low temperature hydrothermal manganese crust from Saldanha field, Mid-Atlantic Ridge. International MoMAR Implementation Workshop, 7–9 April 2005, Lisbon, Portugal, p. 29.

Dias, A.S., Mills, R.A., Taylor, R.N., Ferreira, P., Barriga, F.J.A.S., 2008. Geochemistry of a sediment push-core from the Lucky Strike hydrothermal field, Mid-Atlantic Ridge. Chemical Geology 247 (3–4), 339–351.

Dias, A., Früh-Green, G.L., Bernasconi, S.M., Barriga, F.J.A.S. and teams, S.a.C.D.C., submitted. Geochemistry and stable isotopes constraints on high-temperature activity from sediment cores of the Saldanha field. Marine Geology.

D'Orazio, M., Boschi, C., Brunelli, D., 2004. Talc-rich hydrothermal rocks from the St. Paul and Conrad fracture zones in the Atlantic Ocean. European Journal of Mineralogy 16 (1), 73–83.

Dosso, L., et al., 1999. The age and distribution of mantle heterogeneity along the Mid-Atlantic Ridge (31°–41° N). Earth and Planetary Science Letters 170 (3), 269–286.

Douville, E., et al., 2002. The Rainbow vent fluids (36°14′N, MAR): the influence of ultramafic rocks and phase separation on trace metal content in Mid-Atlantic Ridge hydrothermal fluids. Chemical Geology 184 (1–2), 37–48.

Elderfield, H., Greaves, M.J., 1981. Negative cerium anomalies in the rare earth element patterns of oceanic ferromanganese nodules. Earth and Planetary Science Letters 55 (1), 163–170.

Elderfield, H., Greaves, M.J., 1982. The rare earth elements in seawater. Nature 18, 214–219.

Faure, G., 1986. Principles of Isotope Geology. John Wiley & Sons. 589 pp.

Ferreira, P.L., 2006. Melt supply and magmatic evolution at a large central MOR volcano located in the Lucky Strike segment, 37°N on the Mid-Atlantic Ridge, Azores region. PhD Thesis, University of Southampton, Southampton, 386 pp.

Fouquet, Y., et al., 1997. Discovery and first submergible investigations on the Rainbow hydrothermal field on the MAR (36° 14N). Eos, Transactions, American Geophysical Union 78 (F832).

Fouquet, Y., et al., 1998. FLORES diving cruise with the Nautile near Azores — first dives on Rainbow field: hydrothermal seawater/mantle interaction. Inter Ridge News 7 (1), 1998.

German, C.R., 1998. Hydrothermal scavenging of rare-earth elements in the ocean. Nature 345, 516–518.

German, C.R., et al., 1993. A geochemical study of metalliferous sediment from the TAG hydrothermal mound, 26°08′N, Mid-Atlantic Ridge. Journal of Geophysical Research 98 (B6), 9683–9692.

German, C.R., Parson, L.M., Team, H.S., 1996. Hydrothermal exploration near the Azores Triple Junction: tectonic control of venting at slow-spreading ridges? Earth and Planetary Science Letters 138, 93–104.

German, C.R., Hergt, J., Palmer, M.R., Edmond, J.M., 1999. Geochemistry of a hydrothermal sediment core from the OBS vent-field, 21°N East Pacific Rise. Chemical Geology 155 (1–2), 65–75.

Godfrey, L.V., Mills, R., Elderfield, H., Gurvich, E., 1994. Lead behavior at the Tag hydrothermal vent field, 26°N, Mid-Atlantic Ridge. Marine Chemistry 46 (3), 237–254.

Goldberg, E.D., Koide, M., Bowen, R.A., Smith, R.H., 1963. Rare-earth distribution in the marine environment. Journal of Geophysical Research 68 (14), 4209–4217.

Gràcia, E., Charlou, J.-L., Radford-Knoery, J., Parson, L., 2000. Non-transform offset along the Mid-Atlantic ridge south of the Azores (38°N–34°N): ultramafic exposures and hosting of hydrothermal vents. Earth and Planetary Science Letters 177, 89–103.

Gruau, G., Bernard-Griffiths, J., Lecuyer, C., 1998. The origin of U-shaped rare earth patterns in ophiolite peridotites: assessing the role of secondary alteration and melt/rock reaction. Geochimica et Cosmochimica Acta 62 (21–22), 3545–3560.

Hart, S.R., 1984. A large-scale isotope anomaly in the Southern Hemisphere mantle. Nature 309 (5971), 753–757.

Holm, N.G., Charlou, J.L., 2001. Initial indications of abiotic formation of hydrocarbons in the Rainbow ultramafic hydrothermal system, Mid-Atlantic Ridge. Earth and Planetary Science Letters 191 (1–2), 1–8.

Janecky, D.R., Seyfried, W.E., 1986. Hydrothermal serpentinization of peridotite within the oceanic-crust — experimental investigations of mineralogy and major element chemistry. Geochimica et Cosmochimica Acta 50 (7), 1357–1378.

Kelley, D.S., et al., 2001. An off-axis hydrothermal vent field near the Mid-Atlantic Ridge at 30°N. Nature 412, 445–449.

Klein, F., Bach, W.G., 2009. Fe–Ni–Co–O–S phase relations in peridotite–seawater interactions. Journal of Petrology 50 (1), 37–59.

Klinkhammer, C.P., Elderfield, H., Edmond, J.M., Mitra, A., 1994. Geochemical implications of rare earth element patterns in hydrothermal fluids from mid-ocean ridges. Geochimica et Cosmochimica Acta 58 (23), 5105–5113.
Krasnov, S.G., et al., 1995. Detailed geological studies of hydrothermal fields in the North Atlantic. In: Parson, L.M., Walker, C.L., Dixon, D.R. (Eds.), Hydrothermal Vents and Processes. Geological Society Special Publication, London, pp. 43–64.
Langmuir, C.H., Bender, J.F., Bence, A.E., Hanson, G.N., Taylor, S.R., 1977. Petrogenesis of basalts from famous area — Mid-Atlantic Ridge. Earth and Planetary Science Letters 36 (1), 133–156.
Lowell, R.P., Rona, P.A., 2002. Seafloor hydrothermal systems driven by the serpentinization of peridotite. Geophysical Research Letters 29 (11), 1–4.
Marques, A.F.A., Barriga, F., Chavagnac, V., Fouquet, Y., 2006. Mineralogy, geochemistry, and Nd isotope composition of the Rainbow hydrothermal field, Mid-Atlantic Ridge. Mineralium Deposita 41 (1), 52–67.
McDonough, W.F., Frey, F.A., 1989. Rare earth elements in upper mantle rocks. In: Lipin, B.R., McKay, G.A. (Eds.), Reviews in Mineralogy. Mineralogical Society of America, pp. 100–145.
Melcher, F., Meisel, T., Puhl, J., Koller, F., 2002. Petrogenesis and geotectonic setting of ultramafic rocks in the Eastern Alps: constraints from geochemistry. Lithos 65 (1–2), 69–112.
Mevel, C., 2003. Serpentinization of abyssal peridotites at mid-ocean ridges. Comptes Rendus Geosciences 335 (10–11), 825–852.
Michard, A., 1989. Rare earth element systematic in hydrothermal fluids. Geochimica et Cosmochimica Acta 53, 745–750.
Michard, A., Albarède, F., 1986. The REE contents of some hydrothermal fluids. Chemical Geology 55, 51–60.
Mills, R.A., Elderfield, H., 1995. Rare earth element geochemistry of hydrothermal deposits from the active TAG Mound, 26°N Mid-Atlantic Ridge. Geochimica et Cosmochimica Acta 95 (17), 3511–3524.
Mills, R., Elderfield, H., Thompson, J., 1993. A dual origin for the hydrothermal component in a metalliferous sediment core from the Mid-Atlantic Ridge. Journal of Geophysical Research 98 (B6), 9671–9682.
Mills, R., Wells, D.M., Roberts, S., 2001. Genesis of ferromanganese crusts from the TAG hydrothermal field. Chemical Geology 176, 283–293.
Miranda, J.M., et al., 2003. Study of the Saldanha massif (MAR, 36°34′N): constrains from rock magnetic and geophysical data. Marine Geophysical Research 23, 299–318.
Nakamura, K., et al., 2009. Serpentinized troctolites exposed near the Kairei Hydrothermal Field, Central Indian Ridge: insights into the origin of the Kairei hydrothermal fluid supporting a unique microbial ecosystem. Earth and Planetary Science Letters 280 (1–4), 128–136.
O'Hanley, D.S., 1992. Solution to the volume problem in serpentinization. Geology 20, 705–708.
Paulick, H., et al., 2006. Geochemistry of abyssal peridotites (Mid-Atlantic Ridge, 15° 20′ N, ODP Leg 209): implications for fluid/rock interaction in slow spreading environments. Chemical Geology 234 (3–4), 179–210.
Piepgras, D.J., Jacobsen, S.B., 1992. The behavior of rare earth elements in seawater: precise determination of variations in the North Pacific water column. Geochimica et Cosmochimica Acta 56 (5), 1851–1862.
Prinzhofer, A., Allegre, C.J., 1985. Residual peridotites and the mechanisms of partial melting. Earth and Planetary Science Letters 74 (2–3), 251–265.
Ribeiro da Costa, I., 2005. Serpentinization on the Mid-Atlantic Ridge: the Rainbow, Saldanha and Menez Hom sites. PhD Thesis, Faculdade de Ciências da Universidade de Lisboa, Lisbon, 444 pp.
Savov, I.P., Ryan, J.G., D'Antonio, M., Kelley, K., Mattie, P., 2005. Geochemistry of serpentinized peridotites from the Mariana Forearc Conical Seamount, ODP Leg 125: implications for the elemental recycling at subduction zones. Geochemistry Geophysics Geosystems 6, Q04J15.
Schilling, J.G., 1975. Azores mantle blob: rare-earth evidence. Earth and Planetary Science Letters 25 (2), 103–115.
Schilling, J.G., et al., 1983. Petrologic and geochemical variations along Mid-Atlantic Ridge from 29°N to 73°N. American Journal of Science 283, 510–586.
Schroeder, T., John, B., Frost, B.R., 2002. Geologic implications of seawater circulation through peridotite exposed at slow-spreading mid-ocean ridges. Geology 30, 367–370.
Seyfried Jr., W.E., Foustoukos, D.I., Fu, Q., 2007. Redox evolution and mass transfer during serpentinization: an experimental and theoretical study at 200 °C, 500 bar with implications for ultramafic-hosted hydrothermal systems at Mid-Ocean Ridges. Geochimica et Cosmochimica Acta 71 (15), 3872–3886.
Sharma, M., Wasserburg, G.J., 1996. The neodymium isotopic compositions and rare earth patterns in highly depleted ultramafic rocks. Geochimica et Cosmochimica Acta 60 (22), 4537–4550.
Shaw, D.M., 1970. Trace element fractionation during anatexis. Geochimica et Cosmochimica Acta 34 (2), 237.
Sinha, M.C., Dzhatieva, Z., Dias, A., Fredrichs, N., 2006. RRS Charles Darwin Cruise 167, 23 Nov–21 Dec 2004. Sub-seafloor Physical Properties at Saldanha Seamount, Mid-Atlantic Ridge, and Controls on the Spatial Distribution of Hydrothermal Venting. National Oceanography Centre Southampton, Southampton, UK.
Snow, J.E., Dick, H.J.B., 1995. Pervasive magnesium loss by marine weathering of peridotite. Geochimica et Cosmochimica Acta 59 (20), 4219–4235.
Sugisaki, R., et al., 1983. Origin of hydrogen and carbon-dioxide in fault gases and its relation to fault activity. Journal of Geology 91 (3), 239–258.
Sverjensky, D.A., 1984. Europium redox equilibria in aqueous solution. Earth and Planetary Science Letters 67 (1), 70–78.
Tanaka, T., et al., 2000. JNdi-1: a neodymium isotopic reference in consistency with LaJolla neodymium. Chemical Geology 168 (3–4), 279–281.
Taylor, S.R., McLennan, S.M., 1985. The Continental Crust: its Composition and Evolution: An Examination of the Geochemical Record Preserved in Sedimentary Rocks. Blackwell Science Inc, Oxford.
Thirlwall, M.F., 2000. Inter-laboratory and other errors in Pb isotope analyses investigated using a $^{207}Pb$–$^{204}Pb$ double spike. Chemical Geology 163 (1–4), 299–322.
von Blanckenburg, F., O'Nions, R.K., Hein, J.R., 1996. Distribution and sources of pre-anthropogenic lead isotopes in deep ocean water from Fe–Mn crusts. Geochimica et Cosmochimica Acta 60 (24), 4957–4963.
Wetzel, L.R., Shock, E.L., 2000. Distinguishing ultramafic- from basalt-hosted submarine hydrothermal systems by comparing calculated vent fluid compositions. Journal of Geophysical Research-Solid Earth 105 (B4), 8319–8340.
Wildeman, T.R., Haskin, L.A., 1965. Rare-earth elements in ocean sediments. Journal of Geophysical Research 70 (12), 2905–2910.
Workman, R.K., Hart, S.R., 2005. Major and trace element composition of the depleted MORB mantle (DMM). Earth and Planetary Science Letters 231 (1–2), 53–72.